Mon. Not. R. Astron. Soc. **395,** 328–334 (2009) doi:10.1111/j.1365-2966.2009.14509.x

The unusual X-ray light curve of GRB 080307: the onset of the afterglow?

K. L. Page,[1⋆] R. Willingale,[1] P. T. O'Brien,[1] N. R. Tanvir,[1] J. P. Osborne,[1] B. Zhang,[2] S. T. Holland,[3,4] A. J. Levan,[5] A. Melandri,[6] R. L. C. Starling,[1] D. Bersier,[6] D. N. Burrows,[7] J. E. Geach[8] and P. Maxted[9]

[1]*X-Ray and Observational Astronomy Group, Department of Physics and Astronomy, University of Leicester, Leicester LE1 7RH*
[2]*Department of Physics, University of Nevada, Las Vegas, NV 89154, USA*
[3]*NASA Goddard Space Flight Center, Greenbelt, MD 20771, USA*
[4]*Universities Space Research Association 10211 Wincopin Circle, Suite 500, Columbia, MD 21044-3432, USA*
[5]*Department of Physics, University of Warwick, Coventry CV4 7AL*
[6]*Astrophysics Research Institute, Liverpool John Moores University, Twelve Quays House, Birkenhead CH41 1LD*
[7]*Department of Astronomy and Astrophysics, Pennsylvania State University, State College, PA 16802, USA*
[8]*Department of Physics, Durham University, Durham DH1 3LE*
[9]*Astrophysics Group, Keele University, Keele ST5 5BG*

Accepted 2009 January 15. Received 2009 January 15; in original form 2008 December 15

ABSTRACT

Swift-detected GRB 080307 showed an unusual smooth rise in its X-ray light curve around 100 s after the burst, at the start of which the emission briefly softened. This 'hump' has a longer duration than is normal for a flare at early times and does not demonstrate a typical flare profile. Using a two-component power-law-to-exponential model, the rising emission can be modelled as the onset of the afterglow, something which is very rarely seen in *Swift*-X-ray light curves. We cannot, however, rule out that the hump is a particularly slow early-time flare, or that it is caused by upscattered reverse shock electrons.

Key words: radiation mechanisms: non-thermal – gamma-rays: bursts – X-rays: individual: GRB 080307.

1 INTRODUCTION

Although many gamma-ray burst (GRB) X-ray light curves roughly follow a 'canonical' decay of initially steep and then flat (the so-called 'plateau' phase), before settling into a classical power-law decline phase (see e.g. Nousek et al. 2006; Zhang et al. 2006), some are noticeably different. Examples include GRB 060105, which had an unusually shallow initial decay (Godet et al. 2008); GRB 060218, which was clearly associated with supernova SN 2006aj and showed the breakout of a shock wave from the exploding progenitor (Campana et al. 2006); GRB 061007, where the X-ray decay continued with no breaks until at least 10^6 s after the trigger (Mundell et al. 2007; Schady et al. 2007); GRB 070110, which showed an abrupt drop in the X-ray emission at the end of the 'plateau' stage (Troja et al. 2008). It is examples such as these, whose behaviour differs from those of more typical afterglows, which provide further insight into the physics of the bursts, allowing the testing of models for the early stages of GRB afterglows.

GRB 080307 has a very unusual X-ray light curve, reminiscent of GRB 060218. The emission rose smoothly until about 200 s after the trigger, at which point a long, steady decay set in, continuing unbroken until the afterglow could no longer be detected after a few 10^5 s. Here we show that, in contrast to GRB 060218, the early emission peak is probably the rising afterglow emission; there is no evidence for a supernova shock breakout.

The observations are described in Section 2, with details on the *Swift* spectral analysis and results in Sections 3.1–3.3; ground-based optical follow-up findings are given in Section 3.4. Section 4 presents a discussion.

⋆E-mail: kpa@star.le.ac.uk

2 OBSERVATIONS

2.1 *Swift*

Following the Burst Alert Telescope (BAT) trigger at 11:23:30 UT on 2008 March 7, *Swift* (Gehrels et al. 2004) immediately slewed to the burst and started collecting X-ray Telescope (XRT; Burrows et al. 2005) and UV/Optical Telescope (UVOT; Roming et al. 2005) data at T+99 and T+105 s, respectively. The XRT centroided onboard, though a refined position was quickly determined from the promptly downlinked Single Pixel Event Report (SPER) data (Holland et al. 2008a). The most accurate *Swift* position was later calculated by using the XRT–UVOT alignment and matching UVOT field sources to the USNO-B1 catalogue (see Goad et al. 2007b for more details): RA = $09^{\rm h}06^{\rm m}30\overset{\rm s}{.}72$, Dec. = $+35^\circ08'20\overset{''}{.}3$ (J2000; 90 per cent confidence radius of 1.8 arcsec; Goad et al. 2008).

The data were processed with the standard *Swift* FTOOLS, using v2.8 of the software (release date 2007 December 6) and the corresponding calibration files. The XRT stayed in windowed timing (WT) mode until around 614 s after the trigger, at which point the count rate dropped below 2 count s^{-1} and the XRT automatically switched to photon counting (PC) mode. The PC data obtained towards the end of the first orbit were piled-up, so the light curve and spectrum were extracted using an annulus to exclude the central 4 pixel of the point spread function [PSF; the exclusion radius was estimated by fitting the wings of the PSF with the known King function parameters (Moretti et al. 2005) and determining at which point the observed profile deviated from the expected model]. A comparison of ancillary response files with and without the PSF correction provided the factor by which the count rate needed to be scaled to account for the counts excluded by the annulus.

2.2 Ground-based follow-up

Optical observations were made with Gemini Multi-Object Spectrograph (GMOS) on Gemini North (Tanvir 2008), the Auxilliary Port Camera on the William Herschel Telescope (WHT/AUX) and the 2-m Faulkes Telescope South (FTS). United Kingdom Infrared Telescope/Wide Field Camera (UKIRT/WFCAM) also observed and detected the afterglow in the IR; in this case, a sequence of exposures was obtained, cycling through the filters *JHJKJHJ*, until the target hit the altitude limit of the telescope.

The optical and near-IR magnitudes measured are provided in Table 1; these have not been corrected for the reddening of $E(B-V) = 0.03$ mag (Schlegel, Finkbeiner & Davis 1998). UKIRT magnitudes were calibrated against 15 Two Micron All Sky Survey (2MASS) stars in the field. The WHT and FTS-i' data were calibrated using the Sloan Digital Sky Survey (SDSS) system (Cool et al. 2008), while the USNOB1-0 catalogue was used for the *B* and *R* Bessell filters (Monet et al. 2003).

Table 1. Optical and near-IR measurements. No correction for the expected extinction corresponding to a reddening of $E(B-V) = 0.03$ mag has been made.

Filter	Magnitude	Time (min since burst)	Telescope
B	>21.3 (5σ)	36.2	FTS
r	24.05 ± 0.22	630	WHT
	24.43 ± 0.11	36 560	WHT
	24.10 ± 0.25	76 896	WHT
R	21.60 ± 0.25	22.2	FTS
	22.02 ± 0.47	52.1	FTS
i	22.28 ± 0.03	89	Gemini
	22.32 ± 0.03	93	Gemini
	22.38 ± 0.03	97	Gemini
	22.36 ± 0.03	101	Gemini
	22.38 ± 0.03	105	Gemini
	23.66 ± 0.19	640	WHT
	24.34 ± 0.26	36640	WHT
i'	20.46 ± 0.17	34.78	FTS
J	19.74 ± 0.10	44	UKIRT
	19.96 ± 0.11	54	UKIRT
	20.74 ± 0.22	64	UKIRT
	20.24 ± 0.29	73	UKIRT
H	19.41 ± 0.12	49	UKIRT
	19.29 ± 0.13	69	UKIRT
K	18.14 ± 0.08	59	UKIRT

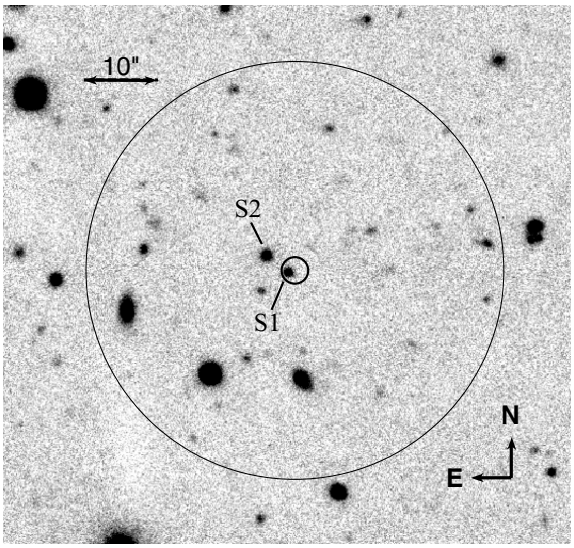

Figure 1. Gemini image, showing the position of the optical afterglow (S1) and the nearby source which was found to contaminate the *Swift*-XRT data (S2). The large circle is the XRT extraction region (radius 28 arcsec).

The Gemini data revealed a faint point source within the revised XRT error circle (Goad et al. 2008), providing an accurate position of RA = $09^{\rm h}06^{\rm m}30\overset{\rm s}{.}80$, Dec. = $+35^\circ08'20\overset{''}{.}1$ (J2000; uncertainty of 0.2 arcsec) for the optical afterglow. Fig. 1 shows the Gemini image (S1 is the position of the afterglow; S2 is the contaminating source discussed below).

2.3 *Chandra*

During an initial inspection of the XRT data, the X-ray light curve showed a break at around 4×10^4 s after the trigger. An apparent very flat decay then continued until the end of the *Swift* observations, around 6×10^6 s (Holland et al. 2008b). Because Gemini optical imaging showed the presence of a nearby object (Fig. 1), just a few arcseconds from the GRB position, we obtained a late-time *Chandra* Target of Opportunity observation in 2008 September, 6.5 months after the burst, to determine whether the slow X-ray decline was intrinsic or due to a contaminating source.

The *Chandra* data did reveal that there was an X-ray source coincident with the optical one, well within the PSF of the XRT. This contaminating source is at a position of RA = $09^{\rm h}06^{\rm m}31\overset{\rm s}{.}04$, Dec. = $+35^\circ08'22\overset{''}{.}4$ (J2000), 3.8 arcsec from the afterglow position (determined from the optical data). Its *i*-band magnitude is ~ 21.85 ($J = 20.67$, $H = 19.88$, $K = 18.93$ from UKIRT observations, with uncertainties of $\sim$0.16 mag), and the X-ray flux is approximately 2.7×10^{-14} erg cm^{-2} s^{-1} (observed; 3.8×10^{-14} erg cm^{-2} s^{-1} unabsorbed). This implies an optical-to-X-ray ratio of $\alpha_{\rm ox} \sim 1.4$, typical for an active galactic nucleus. The afterglow itself was not detected during the *Chandra* pointing.

The flux of the nearby source corresponds to $\sim 8 \times 10^{-4}$ count s^{-1} in the XRT. This value has been subtracted off all the X-ray data points in the light curve.

At the flux level of the contaminating source, the sky density of X-ray sources is about 57 per deg^2 (Mateos et al. 2008). This gives approximately a 1 per cent chance of finding such a source in the extraction region used (radius of 28 arcsec). Given that *Swift* has detected more than 350 GRBs to date, it is likely that other X-ray light curves reaching similar levels have been affected by contaminating sources. A possible example, noted by the authors, is GRB 050422

(Beardmore et al. 2007), which also showed a levelling-off of the light curve at later times.

3 ANALYSIS AND RESULTS

3.1 *Swift*-BAT

The BAT (Barthelmy et al. 2005) data give a T_{90} value of 126 ± 26 s. A spectrum covering this time can be fitted with a single power-law photon index of $\Gamma = 1.81^{+0.24}_{-0.22}$, with no requirement for any form of energy cut-off or break. The corresponding 15–150 keV flux is 6.3×10^{-9} erg cm^{-2} s^{-1}.

Fig. 2 shows the BAT light curves over the standard energy bins (15–25, 25–50, 50–100 and 100–350 keV), while Fig. 3 demonstrates how the γ-ray emission softened during the burst. Fitting spectra for $T = 0$–50 and 50–126 s also shows this trend: $\Gamma_{0-50\,\mathrm{s}} = 1.53 \pm 0.18$ and $\Gamma_{50-125\,\mathrm{s}} = 3.18^{+0.96}_{-0.70}$.

Fig. 2 also shows how the peak of the γ-ray data both moved to later times and broadened at softer energies; this trend continued for the X-ray data. A Gaussian component was applied to each light curve to parametrize the changes in a simple manner and the results are given in Table 2.

3.2 X-ray analysis

3.2.1 Temporal analysis

Excluding the hump in the light curve and fitting the XRT data after 800 s, a single power law is a good fit, with a decay slope of $\alpha = 1.95 \pm 0.10$ (where $F_{\nu,t} \propto \nu^{-\beta} t^{-\alpha}$ and the photon spectral index, $\Gamma = \beta + 1$). After about 2×10^5 s, the afterglow is no longer significantly detected above the nearby source. A slope of $\alpha \sim 1.95$ is more typical of the 'normal' decay phase of the 'canonical' X-ray afterglow (Nousek et al. 2006; Zhang et al. 2006; Evans et al. 2009; Racusin et al. 2009), being significantly steeper than the 'plateau' stage.

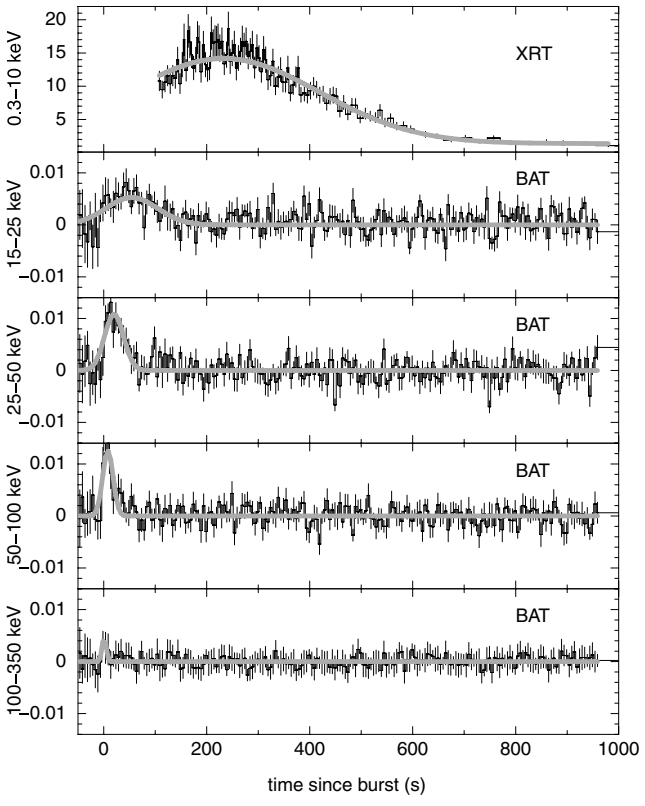

Figure 2. The light-curve peak becomes broader and moves later in time over the softer bands – see Table 2. The model fitted is a Gaussian (together with an underlying power-law decay for the XRT data). The units are count s^{-1} (fully illuminated detector)$^{-1}$ for the BAT and count s^{-1} for the XRT.

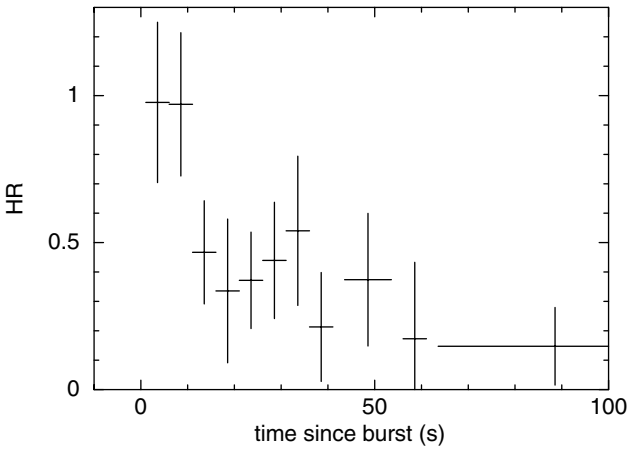

Figure 3. The BAT HR of GRB 080307, showing a spectral softening over the first 100 s of the emission. The HR is defined as the ratio of the counts in the 50–150 and 15–50 keV bands.

Table 2. Gaussian component fitted to each energy band of the *Swift* light curve (Fig. 2). The peak is narrower and occurs earlier at harder energies.

Bandpass (keV)	Gaussian centre (s)	Width (s)
0.3–10	234^{+16}_{-17}	185 ± 15
15–25	54 ± 9	39^{+10}_{-8}
25–50	23^{+5}_{-4}	17^{+5}_{-4}
50–100	$8.6^{+1.5}_{-1.3}$	$6.6^{+1.8}_{-1.3}$
100–350	$1.3^{+2.4}_{-1.0}$	$1.5^{+2.6}_{-0.9}$

The fluence of the hump emission between 100 and 600 s is $\sim 2.1 \times 10^{-7}$ erg cm^{-2}, about a quarter of the time-averaged BAT (15–150 keV) burst fluence measured by Sato et al. (2008).

Fig. 4 compares the hard (1.5–10 keV) and soft (0.3–1.5 keV) light curves, showing there is a softening during the beginning of the brightening phase, after which the hardness ratio (HR) remains close to constant; the data beyond 600 s show no evidence for a change in hardness either. This early behaviour is unusual for a GRB 'flare' or 'pulse': typically, as the count rate increases, so, too, does the hardness (e.g. Golenetskii et al. 1983; Ford et al. 1995; Borgonovo & Ryde 2001; Goad et al. 2007a; Page et al. 2007). However, the start of this rise may not have been caught by the XRT, so there could have been an earlier hardening – and some flares do seem to start hard and then just soften (e.g. GRB 050502B; Falcone et al. 2006). The spectral evolution of flares does tend to continue during the peak and beyond, though, which is not seen in this case; after about 140 s post-trigger, there is little or no further change of spectral shape in GRB 080307.

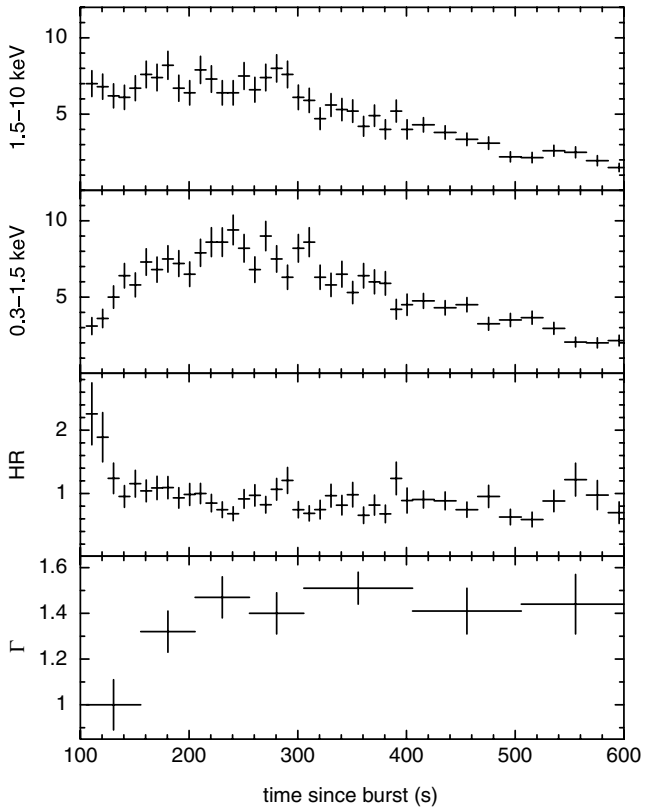

Figure 4. The XRT-WT light curves over 1.5–10 and 0.3–1.5 keV, together with the HR, showing an initial softening until ∼140 s. After this time the HR remains approximately constant. The bottom panel shows the photon indices obtained from fitting the spectra with a single power law.

3.2.2 Spectral analysis

Time-sliced spectra were extracted throughout the hump in the light curve from T_0 + 100–600 s, and the resulting power-law fits are shown in the bottom panel of Fig. 4. The absorbing column was fixed at the Galactic value (2.37×10^{20} cm^{-2}; Kalberla et al. 2005), since no higher $N_{\rm H}$ was suggested by the fit. An alternative fit of keeping the power-law index fixed and allowing the variation of $N_{\rm H}$ to account for the difference in spectral shape did not provide such a good fit (χ^2 was 10 higher, for one fewer degree of freedom).

A spectrum extracted for the PC data from T_0 + 4.4 ks onwards (to avoid any residual emission from the 'flare') has $\Gamma = 1.66 \pm 0.30$. Note, however, that the fit is improved if $N_{\rm H}$ is allowed to vary (99.5 per cent via the F-test), leading to $\Gamma = 2.16^{+0.36}_{-0.33}$, with a total column at $z = 0$ (including the Galactic value) of $N_{\rm H} = (1.8^{+2.2}_{-1.5}) \times 10^{21}$ cm^{-2}. This is discussed further in Section 4.

3.3 *Swift*-UVOT

No afterglow was detected by the UVOT (Roming et al. 2005). Holland (2008) lists the 3σ upper limits, which range between >20.6 and 21.4 for the optical and UV filters (summed over a few hundred to a few thousand seconds after the trigger). The afterglow was also not detected in the broad-bandpass white filter, to a limiting magnitude of >22.3.

3.4 Ground-based follow-up

Gemini detected a faint $i \approx 22.3$ point source approximately 90 min post-trigger (Fig. 1), which faded by about 0.1 mag during the course of this sequence (Table 1). WHT also found a faint blue source approximately 11 h post-burst in r and i filters, although subsequent observations with the WHT over the course of several weeks showed no significant variation in the luminosity of the source, indicating the host galaxy was being detected.

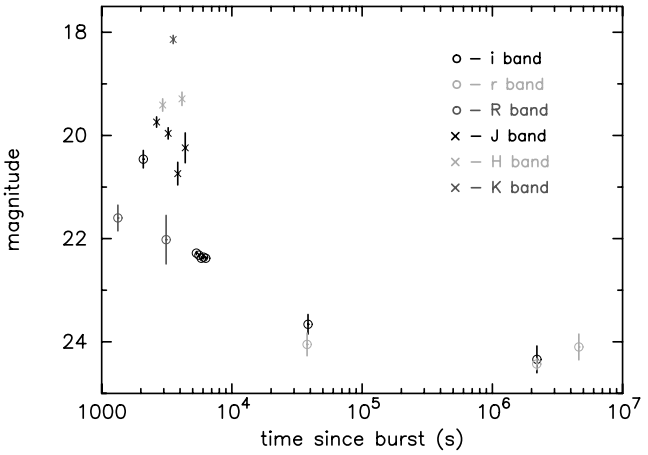

Figure 5. Ground-based optical data obtained using Gemini/GMOS (i band), WHT/AUX (i and r band), FTS (R and i band) and near-IR (J, H and K band) data from UKIRT.

Fig. 5 shows the optical and IR data listed in Table 1. The second UKIRT H-band measurement seems to be slightly in excess of the previous point, and the J-band point around 4.2 ks is above that at ∼3.8 ks. Unfortunately, there are no simultaneous X-ray observations, but the X-ray data at the beginning of the second orbit (∼4.4 ks) do seem to be slightly higher than the underlying power law. It is therefore plausible that there was a similar fluctuation in the X-ray and IR bands around this time.

4 DISCUSSION

4.1 Limits on a supernova component

The late time limit on variability between the final two r-band observations is 0.23 ± 0.22 μJy, corresponding to a 3σ limit on any variable source of 0.66 μJy, or an $r \sim 24.4$ source, which we take to be the limit of any supernova present at the time of our intermediate r-band observations (roughly 25 d post-burst in the observer frame). Comparing this to redshifted light curves of SN 1998bw (Galama et al. 1998), we determine that we would have observed a brightening due to a supernova component akin to SN 1998bw should it have been located at $z \lesssim 0.7$. This could be reduced if there were to be significant foreground extinction in the direction of GRB 080307. The moderately red $R - K$ colour ($R - K \sim 4$) suggests this may be the case, although there is no strong evidence for excess $N_{\rm H}$ from the X-ray data (see Section 4.3); thus, the lack of SN component does not place strong constraints on the redshift.

4.2 Possible constraints on the redshift

The lack of variation in the WHT data implies that those observations are dominated by the host galaxy. The absence of a supernova makes it unlikely that this burst occurred at low redshift [very high foreground extinction ($A_V \sim 4$–5 for a burst at $z = 0.1$) would be required], despite the resemblance between this light curve and that

of the low-z GRB 060218 (Campana et al. 2006), whilst the magnitude of the host galaxy is entirely consistent with many other GRB hosts at $z \lesssim 2$ (see e.g. Savaglio, Glazebrook & Le Borgne 2008).

Ukwatta et al. (2008) have investigated certain BAT parameters which may indicate when a burst is at a high redshift. Based on a limited sample of bursts, there are four criteria which together imply an 85 per cent chance of a GRB having a redshift greater than 3.5; GRB 080307 fulfils these four points. Note, though, that the most distant GRB yet measured (GRB 080913; Greiner et al. 2008) did not satisfy all these criteria.

The XRT data from the second orbit onwards, when no spectral evolution is apparent and the light curve is following a steady decline, gave an indication of an absorbing column in excess of the Galactic value of $N_{\rm H} \sim 1.6 \times 10^{21}\,{\rm cm}^{-2}$ (at $z = 0$); this is quite poorly constrained, however. This excess implies an upper limit on the redshift of $z \lesssim 3.8$ according to the method of Grupe et al. (2007a), though this increases to $z \lesssim 6.5$ using the lower limit on the excess column. This is in comparison to the lower limit estimate of $z \gtrsim 3.5$ as indicated by the BAT data (Section 3.1), although the detection of the host galaxy makes it unlikely that the burst occurred at such a redshift.

4.3 Spectral anomalies

If the additional column of $N_{\rm H} \sim 1.6 \times 10^{21}\,{\rm cm}^{-2}$ is used when fitting time-sliced data through the hump, it is found that a single power law is a poor fit, with a much softer component (either a second power law, or a blackbody) being required as well. The 'underlying' power law still shows the softening trend plotted in Fig. 4, though.

GRB 060218 showed a similar rise in its early X-ray light curve, and it was found that the spectra during this interval showed evidence for an expanding thermal component, corresponding to a supernova shock breakout (Campana et al. 2006). Fitting a similar model here, however, results in the temperature and radius of the blackbody component remaining approximately constant throughout ($kT \sim 130$–$140\,{\rm eV}$ and an emitting radius of $\sim 200 D_{10\,{\rm kpc}}\,{\rm km}$, where $D_{10\,{\rm kpc}}$ is the distance from the observer to the burst in units of 10 kpc), making it inconsistent with a shock breakout (a cooling temperature and expanding radius would be expected). No supernova has been identified for GRB 080307 either. It therefore seems unlikely that a thermal component is the explanation for the possible spectral curvature. A dual power-law model can equally well fit the spectrum, with photon indices of $\Gamma \sim 3$ and ~ 1 (both initially softening). Moretti et al. (2008) investigated additional spectral components in a sample of soft X-ray afterglow spectra. Their extra component was required to model an excess at higher energies, though, and there were no obvious humps in the light curves, although there is some possible curvature in GRB 061110A (see http://www.swift.ac.uk/xrt_curves/00238109; Evans et al. 2007, 2009).

The excess absorbing column in GRB 080307 is not strongly significant, however, and no obvious explanation presents itself for multiple components. Thus, we simply mention this other unusual feature in passing and accept that there are residual uncertainties in the measurement of excess absorption.

4.4 Light curve

The X-ray light curve of GRB 080307 showed an unusual hump starting around 100 s after the burst. Below a number of possible explanations are considered.

4.4.1 Flare

The XRT light curve can be modelled as a single, unbroken power-law decay (with a large, superimposed hump), with no evidence for the series of breaks often found in the light curves of X-ray afterglows (e.g. Nousek et al. 2006; Zhang et al. 2006). It is relatively unusual for a promptly observed X-ray afterglow to follow a single decay, with only about 15 per cent of *Swift* XRT light curves showing no breaks before 100 ks (Evans et al. 2009).

Flares in X-ray afterglows have a typical relative width of $\langle \Delta t/t \rangle = 0.31 \pm 0.24$ (Chincarini et al. 2007), where Δt is the full width at half-maximum (FWHM $= 2.3548\sigma$, where σ, the Gaussian standard deviation width, is the number used in the Chincarini paper) and t is the time of the flare. The longest relative width in the Chincarini sample was $\Delta t/t = 1.27$ for GRB 051117A (Goad et al. 2007a), whereas GRB 080307 has $\Delta t/t \sim 1.48$. The rising emission at the start of the X-ray light curve of GRB 080307 has a much longer duration than is typical for such an early time relative to the trigger. The other measurement of interest is the relative flux variability, $\Delta F/F$, which compares the flux at the peak of the 'flare' to that of the underlying power law. In the case of GRB 080307, the values for $\Delta t/t$ and $\Delta F/F$ (1.48 and 6.17, respectively) lie in the patchy shells regime [see fig. 1 in Ioka, Kobayashi & Zhang (2005) or fig. 16 in Chincarini et al. (2007)], though could also be caused by refreshed shocks.

4.4.2 Reverse shock

Kobayashi et al. (2007) discuss how synchrotron self-inverse Comptonization (SSC) can cause electrons in the reverse shock region to be upscattered into the X-ray regime (reverse shocks are typically expected to radiate photons in the optical or IR bands). They show that SSC emission can lead to an X-ray flare around the deceleration time using GRB 050406 (Romano et al. 2006) as an example. In such a case there needs to be a steep transition from the reverse shock to the forward one ($\sim t^{-(3p+1)/3}$ from fig. 2 of Kobayashi et al.), but this decay phase could be very short, so can be accommodated by our data.

Reverse shock emission can only explain single flares and, in the thick shell case, is expected to overlap in time with the prompt emission. Fig. 6 demonstrates that the X-ray emission in question does follow on from the BAT detection without any obvious gap, and thus reverse shock SSC emission is a possible origin of the hump seen in this burst.

4.4.3 Onset of afterglow

Instead of considering the initial X-ray rise as being a flare, however, it could be thought of as the onset of the afterglow – something which was expected to be seen in the pre-*Swift* era (e.g. Sari & Piran 1999a,b; Piro et al. 2005; Molinari et al. 2007; Panaitescu & Vestrand 2008 also discuss rising optical afterglows). The profile of the emission in GRB 080307 is quite smooth, rising gradually, something which is not generally the case for flares formed by internal shocks. Kobayashi & Zhang (2007) also discuss the onset of GRB afterglows, showing that a smooth bump can be produced by the forward shock emission.

Willingale et al. (2007) discuss a method of parametrizing BAT–XRT light curves using one or two exponential-to-power-law functions to model the prompt and afterglow emission; see also O'Brien et al. (2006). If a single function is applied to the data, ignoring the

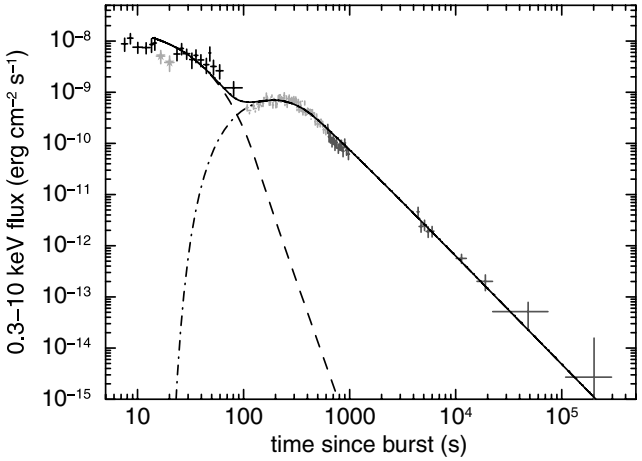

Figure 6. Two exponential-to-power-law components fitted to the BAT–XRT flux light curve. The grey stars indicate points masked out when fitting the model. Black crosses show the BAT data, while the light and dark grey points are WT and PC mode XRT data, respectively. The dashed line is the fit to the prompt emission component, while the dot–dashed one models the afterglow.

broad hump as a flare, the start of the X-ray continuum emission is not well fitted. Fitting one component to account for the prompt (BAT) emission and modelling the increase seen in the XRT as the onset of the afterglow produces a better fit, shown in Fig. 6 (where the BAT data have been extrapolated into the 0.3–10 keV as described in O'Brien et al. 2006); the grey stars indicate data masked out when performing the fit.

The power law starts to dominate the X-ray fit ∼480 s after the trigger, with a decay slope of $\alpha \sim 2.12$. This is of the same order as the $\alpha \sim 1.95$ found in Section 3.2.1. There may be additional curvature during the later decay (after a few 10^4 s), which could be related to deceleration of a thick fireball shell (Kobayashi & Zhang 2007 – see their fig. 7; Lazzati & Begelman 2006).

Very few *Swift*-X-ray light curves show a rising component (other than flares), though most show a slow decline, plateau phase (e.g. Nousek et al. 2006; Zhang et al. 2006). As shown by O'Brien et al. (2006) and Willingale et al. (2007), if the afterglow emission starts while the prompt emission is still bright, the initial rise may be hidden; then, when the prompt component fades sufficiently, the turn-over from the exponential to power-law decay is seen as a 'flat-ish' phase. If the XRT had started observing GRB 080307 even 50 s later, the rising portion would have been missed, and a (short) plateau phase would have been all that was seen at the start of the afterglow; this was the case for GRB 080810 (Page et al., in preparation). Fig. 6 shows that the function modelling the prompt, γ-ray emission drops very suddenly ($\alpha \sim 6$), which may be why the afterglow was prominently visible (i.e. bright with respect to the prompt emission) from an early time. The sample of bursts in Willingale et al. (2007) contains only a small number of bursts with $\alpha_p > 5$. The BAT–XRT light curve of GRB 060427 is plotted in that paper, demonstrating that, had it been a little brighter, the rise of the afterglow would probably have been briefly visible.

Following Molinari et al. (2007), the initial Lorentz factor, Γ_0, can be estimated from the peak time of the afterglow light curve. Here we find that the X-ray light-curve peaks (assuming that this does correspond to the rise of the afterglow) around 234 s (Table 2); this corresponds to the deceleration time. Calculating the fluence over 1–1000 keV in the rest frame to be 2×10^{-6} erg cm^{-2}, we find $\Gamma(t_{\rm peak}) \sim 156(\eta_{0.2} n_0)^{-1/8}\ (1+z)^{3/8}$, where $\eta_{0.2}$ is the radiative efficiency in units of 0.2 and n_0 is the particle density of the (homogenous) surrounding medium in cm^{-3}. Since $\Gamma(t_{\rm dec})$, which is equal to $\Gamma(t_{\rm peak})$ here, is expected to be half of the initial Lorentz factor, $\Gamma_0 = 312(\eta_{0.2} n_0)^{-1/8}\ (1+z)^{3/8}$. For the mean *Swift* redshift of 2.26 (Jakobsson et al. 2006),[1] this corresponds to a value of 486 [assuming typical values of $\eta = 0.2$ and $n = 1$ cm^{-3} from Bloom, Frail & Kulkarni (2003)]. The limit on the redshift from the Grupe et al. $N_{\rm H}$ analysis suggests an upper limit of $\Gamma_0 < 562$.

Swift-XRT light curves do not typically contain smoothly rising features, although flares are seen in about 50 per cent of bursts (e.g. Chincarini et al. 2007; Falcone et al. 2007). Utilizing the light-curve repository (Evans et al. 2007, 2009), we find there are a small number of bursts where a possible early rise is seen which does not look like a standard flare (e.g. GRB 070328 – Markwardt et al. 2007; GRB 070714B – Racusin, Barbier & Landsman 2007; GRB 080205 – Markwardt et al. 2008; GRB 080229A – Cannizzo et al. 2008; GRB 080721 – Marshall et al. 2008). However, in these cases the light curve can be sufficiently well modelled with a series of abruptly broken power laws, rather than requiring a smooth turnover. There are also bursts which show a more gradual roll-over than can be well modelled by a series of broken power laws (GRB 070508 – Grupe et al. 2007b; GRB 080319C – Starling et al., in preparation; GRB 080503 – Mao et al. 2008; GRB 080523 – Stroh et al. 2008; GRB 080605 – Sbarufatti et al. 2008). More recently, GRB 081028 (Guidorzi, Margutti & Mao 2008; Schady & Guidorzi 2008) showed smoothly rising emission, but in this case beginning around 10 ks after the trigger time, and reaching a peak about 10 ks later. For this burst, no spectral softening is apparent (see http://www.swift.ac.uk/xrt_curves/00332851). It remains unclear whether these bursts are displaying the same phenomenon as GRB 080307 or are unrelated, however.

5 SUMMARY

GRB 080307 showed a long, smooth hump early in its X-ray afterglow light curve. Although superficially similar to the supernova shock breakout of GRB 060218, in this case no evidence for radial expansion was seen. The hump is unique in the *Swift* data set, although may possibly be less well observed in a few other bursts. We have considered various origins for the hump: a flare due to a patchy shell or a refreshed shock, reverse shock SSC and the onset of the afterglow.

The long duration of the hump would make this a very slow flare for early times and the spectral softening seen at the start of the curvature is also unusual for a flare. In the case of the reverse shock interpretation, the transition to the forward shock would have to be very short to be hidden within the data. All of these mechanisms are viable explanations of the observed properties, however, the onset of the X-ray afterglow remains a natural interpretation.

ACKNOWLEDGMENTS

The authors acknowledge support for this work at the University of Leicester by STFC. We thank Gordon Stewart for advice regarding the sky density of faint X-ray sources and the referee for helpful comments which improved the paper.

[1] The mean redshift given in the paper has been updated at http://raunvis.hi.is/∼pja/GRBsample.html

REFERENCES

Barthelmy S. D. et al., 2005, Space Sci. Rev., 120, 143
Beardmore A. P. et al., 2007, MNRAS, 374, 1473
Bloom J. S., Frail D. A., Kulkarni S. R., 2003, ApJ, 594, 674
Borgonovo L., Ryde F., 2001, ApJ, 548, 770
Burrows D. N. et al., 2005, Space Sci. Rev., 120, 165
Campana S. et al., 2006, Nat, 442, 1008
Cannizzo J. K. et al., 2008, GCN Rep., 119.2
Chincarini G. et al., 2007, ApJ, 671, 1903
Cool R. J. et al., 2008, GCN Circ., 7372
Evans P. A. et al., 2007, A&A, 469, 379
Evans P. A. et al., 2009, MNRAS, submitted
Falcone A. D. et al., 2006, ApJ, 641, 1010
Falcone A. D. et al., 2007, ApJ, 671, 1921
Ford L. A. et al., 1995, ApJ, 439, 307
Galama T. J. et al., 1998, Nat, 395, 670
Gehrels N. et al., 2004, ApJ, 611, 1005
Goad M. R. et al., 2007a, A&A, 468, 103
Goad M. R. et al., 2007b, A&A, 476, 1401
Goad M. R., Goad M. R., Osborne J. P., Beardmore A. P., Evans P. A., 2008, GCN Circ., 7366
Godet O. et al., 2006, A&A, 452, 819
Godet O. et al., 2008, A&A, submitted
Golenetskii S. V., Mazets E. P., Aptekar R. L., Ilinskii V. N., 1983, Nat, 306, 451
Greiner J. et al., 2008, ApJ, in press (arXiv:0810.2314)
Grupe D., Nousek J. A., van den Berk D. E., Roming P. W. A., Burrows D. N., Godet O., Osborne J., Gehrels N., 2007a, AJ, 133, 2216
Grupe D. et al., 2007b, GCN Rep., 54.2
Guidorzi C., Margutti R., Mao J., 2008, GCN Circ., 8429
Holland S. T., 2008, GCN Circ., 7375
Holland S. T. et al., 2008a, GCN Circ., 7362
Holland S. T., Sato G., Palmer D. M., Page K. L., 2008b, GCN Rep., 131.1
Immler S. et al., 2008, ApJ, 674, L85
Ioka K., Kobayashi S., Zhang B., 2005, ApJ, 631, 429
Jakobsson P. et al., 2006, A&A, 447, 897
Kalberla P. M. W., Burton W. B., Hartmann D., Arnal E. M., Bajaja E., Morras R., Pöppel W. G. L., 2005, A&A, 440, 775
Kobayashi S., Zhang B., 2007, ApJ, 655, 973
Kobayashi S., Zhang B., Mészáros P., Burrows D., 2007, ApJ, 655, 391
Lazzati D., Begelman M. C., 2006, ApJ, 641, 972
Liang E. W., Racusin J. L., Zhang B., Zhang B.-B., Burrows D. N., 2008, ApJ, 675, 528
Mao J., Guidorzi C., Ukwatta T., Brown P. J., Barthelmy S. D., Burrows D. N., Roming P., Gehrels N., 2008, GCN Rep., 138.1
Markwardt C. B., Evans P. A., Goad M., Marshall F. E., 2007, GCN Rep., 42.3
Markwardt C. B., Starling R., Oates S., Barthelmy S. D., Burrows D. N., Roming P., Gehrels N., 2008, GCN Rep., 112.1
Marshall F. E., Guidorzi C., Ward P. A., Barthelmy S. D., Burrows D. N., Roming P., Gehrels N., 2008, GCN Rep., 156.1
Mateos S. et al., 2008, A&A, 492, 51
Molinari E. et al., 2007, A&A, 469, L13
Monet D. G. et al., 2003, AJ, 125, 984
Moretti A. et al., 2005, in Siegmund O. H. W., ed., Proc. SPIE, Vol. 5898, UV, X-Ray and Gamma-Ray Space Instrumentation for Astronomy XIV. SPIE, Bellingham, p. 348
Moretti A. et al., 2008, A&A, 478, 409
Mundell C. G. et al., 2007, ApJ, 660, 489
Nousek J. A. et al., 2006, ApJ, 642, 389
O'Brien P. T. et al., 2006, ApJ, 647, 1213
Page K. L. et al., 2007, ApJ, 663, 1125
Panaitescu A., Vestrand W. T., 2008, MNRAS, 387, 497
Piro L. et al., 2005, ApJ, 623, 314
Racusin J., Barbier L., Landsman W., 2007, GCN Rep., 70.1
Racusin J. et al.2009, ApJ, submitted (arXiv:0812.4780)
Romano P. et al., 2006, A&A, 450, 59
Roming P. W. A. et al., 2005, Space Sci. Rev., 120, 95
Sari R., Piran T., 1999a, ApJ, 520, 641
Sari R., Piran T., 1999b, A&AS, 138, 537
Sato G. et al., 2008, GCN Circ., 7373
Savaglio S., Glazebrook K., Le Borgne D., 2008, ApJ, 691, 182
Sbarufatti B. et al., 2008, GCN Rep., 142.1
Schady P., Guidorzi C., 2008, GCN Circ., 8431
Schady P. et al., 2007, MNRAS, 380, 1041
Schlegel D. J., Finkbeiner D. P., Davis M., 1998, ApJ, 500, 525
Stroh M. C. et al., 2008, GCN Circ., 7767
Tanvir N. R., 2008, GCN Circ., 7369
Troja E. et al., 2007, ApJ, 665, 599
Ukwatta T. N., Sakamoto T., Stamatikos M., Gehrels N., Dhuga K. S., 2008, in Galassi M., Palmer D., Fenimore E., eds, Proc. Santa Fe Conf., AIPC 1000, Gamma-Ray Bursts 2007. Am. Inst. Phys., New York, p. 166
Willingale R. et al., 2007, ApJ, 662, 1093
Zhang B., Mészáros P., 2004, Int. J. Mod. Phys. A, 19, 2385
Zhang B., Fan Y. Z., Dyks J., Kobayashi S., Mészáros P., Burrows D. N., Nousek J. A., Gehrels N., 2006, ApJ, 642, 354
Ziaeepour H. et al., 2008, MNRAS, 385, 453

This paper has been typeset from a TEX/LATEX file prepared by the author.